LIQUID CRYSTALS, 1989, VOL. 5, NO. 2, 699–715

Invited Lecture

New results on the electrohydrodynamic instability in nematics

by L. KRAMER, E. BODENSCHATZ, W. PESCH, W. THOM and W. ZIMMERMANN

Physikalisches Institut der Universität Bayreuth, D-8580 Bayreuth, F.R. Germany

We present theoretical results on the threshold and near-threshold behaviour of electrohydrodynamic convection of planarly aligned nematics under D.C. and A.C. driving. We use the general three dimensional description and include the flexoelectric effect. The experimentally established threshold behaviour is captured in many cases quantitatively, an exception being the extended travelling patterns. Slightly above threshold the observed undulated rolls pose some problems. Defect-mediated turbulence can presumably be explained by mean-flow effects.

1. Introduction

When an alternating voltage is applied across a thin layer of nematic liquid crystal with negative (or slightly positive) dielectric anisotropy ε_a, sufficient (ionic) conductivity and uniform orientation of the director $\hat{\mathbf{n}}$ in the plane of the layer, an instability of the basic unstructured state occurs which, under ideal conditions, leads to a periodic pattern of convection rolls connected with periodic distortions of the director (for reviews see [1–3]). There is a sharp and reversible threshold for this phenomenon which, at low frequencies, is typically between 5 and 10 V. When the voltage is increased further transitions are found to more complicated spatio-temporal states which are usually heavily influenced by defects and often exhibit irregular motion (weak turbulence) [4–6]. If the increase in voltage is performed adiabatically slowly and the conditions are sufficiently ideal, well defined secondary transitions to essentially perfect structures, which in most cases are periodic in two directions, can sometimes be observed [7, 8]. At sufficiently high voltage a transition to strong turbulence occurs (often called the dynamic scattering mode).

This electrohydrodynamic convection (EHC) in nematics, which was discovered about 25 years ago and was intensely studied until about 1975, has received renewed interest in recent years. One of the reasons for this is the present general interest in pattern-forming systems (see, for example [9, 10]). In this context EHC has some unique features. Due to the small thickness of the layers (usually 5–200 μm) the relaxation times are short and specimens can easily be produced with large aspect ratio (ratio of lateral dimension to thickness). There are several easily accessible external control parameters and, in principle, a vast variety of nematics with very different material constants so that very rich scenarios can be observed. Planar anchoring of the director at the upper and lower plates provide for an axial anisotropy, so that the pattern orientates with respect to the preferred axis. Unfortunately there is only one material, 4-methoxybenzylidene-4′-*n*-butyl aniline (MBBA) which has $\varepsilon_a < 0$ and for which all the material parameters are known, but this material is chemically rather unstable. Moreover, the theoretical description of EHC is very complicated due to the complexity of the underlying hydrodynamic equations.

0267-8292/89 $3.00 © 1989 Taylor & Francis Ltd

The basic equations used are provided by the standard hydrodynamic description of nematics (see, for example [3]). They consist of momentum balance (Navier–Stokes equation) together with incompressibility $\nabla \cdot \mathbf{v} = 0$, which determine the velocity field $\mathbf{v}$, and the balance of torque which gives the director $\hat{\mathbf{n}}$. Moreover, there are electric field equations in the quasi-static approximation

$$\operatorname{div} \mathbf{D} = \varrho_e, \quad \mathbf{curl}\, \mathbf{E} = \mathbf{0}, \tag{1}$$

$$\mathbf{D} = \boldsymbol{\varepsilon}\mathbf{E} + \mathbf{P}_{\text{flexo}}, \tag{2}$$

$$\operatorname{div} \mathbf{j} + \partial \varrho_e / \partial t = 0, \tag{3}$$

$$\mathbf{j} = \boldsymbol{\sigma}\mathbf{E} + \varrho_e \mathbf{v}. \tag{4}$$

Here the dielectric and conductivity tensors $\boldsymbol{\varepsilon}$ and $\boldsymbol{\sigma}$ are characterized by $\varepsilon_\perp$ and $\varepsilon_\parallel$ (or $\varepsilon_a = \varepsilon_\parallel - \varepsilon_\perp$) and $\sigma_\perp$ and $\sigma_\parallel$, i.e. their components perpendicular and parallel to $\hat{\mathbf{n}}$. The flexoelectric polarization is given by [11, 12]

$$\mathbf{P}_{\text{flexo}} = e_1 \hat{\mathbf{n}}(\nabla \cdot \hat{\mathbf{n}}) + e_3(\hat{\mathbf{n}} \cdot \nabla)\hat{\mathbf{n}}. \tag{5}$$

Equations (1)–(4) couple to the Navier–Stokes equation mainly through the volume force $\varrho_e \mathbf{E}$ and to the torque balance equation through the dielectric and flexoelectric torques. The full set of equations has to be supplemented by appropriate boundary conditions at the upper and lower plates.

The threshold for EHC is calculated by assuming that all quantities deviate only very little from their values in the basic unstructured state, which is characterized by $\mathbf{v} = \mathbf{0}$, $\hat{\mathbf{n}} = \hat{\mathbf{x}}$ (we choose the layer in the xy plane), $\mathbf{E} = (V(t)/d)\hat{\mathbf{z}}$ (V is the externally applied voltage and d is the layer thickness), $\varrho_e = 0$, $\mathbf{j} = \sigma_\perp \mathbf{E}$. We then write $\hat{\mathbf{n}} = (\cos\theta \cos\psi, \cos\theta \sin\psi, \sin\theta)$ and linearize the equations in the small deviations. The resultant set of linear partial differential equations does not depend on x and y explicitly (translational invariance). They thus admit (modal) solutions which are harmonic in x and y and may be chosen proportional to $\sin(qx + py)$ and $\cos(qx + py)$ (wavevector $\mathbf{q} = (q, p)$).

The pressure can be eliminated by taking the curl of the Navier–Stokes equations, and using equations (1) and (3) to eliminate the charge density ϱ_e, and satisfy $\mathbf{curl}\, \mathbf{E} = \mathbf{0}$ by writing

$$\mathbf{E} = -\nabla\phi + (V(t)/d)\hat{z},$$

where ϕ is the induced potential. We consider constant or time-periodic driving voltages $V(t)$ (period $T = 2\pi/\omega$). The temporal behaviour of the modes is then expected to be of the form

$$\begin{aligned} \mathbf{u}(t) &= \bar{\mathbf{u}}(t) \exp \sigma t, \\ \mathbf{u} &= (\phi, \theta, \psi, \mathbf{v}), \\ \sigma &= \sigma' + \mathrm{i}\sigma'', \end{aligned} \tag{6}$$

where $\bar{\mathbf{u}}$ is periodic ($\bar{\mathbf{u}}$ is constant if V is constant; the overbars are omitted from now on) and σ is the Floquet coefficient. We are then left with equations of the general form

$$\mathbf{M}\partial_t \mathbf{u} = \mathbf{L}\mathbf{u}, \tag{7}$$

where the 6×6 matrices $\mathbf{M}$ and $\mathbf{L}$ depend on $V(t)$, $\mathbf{q}$ and σ, and contain derivatives with respect to z (see [3, 15, 18] for an explicit presentation of the set (7)).

The boundary conditions are

$$\mathbf{u} = \mathbf{0} \quad \text{at} \quad z = \pm d/2, \tag{8}$$

(from $\nabla \cdot \mathbf{v} = 0$ we also have $\partial_z v_z = 0$ at $z = \pm d/2$). Here rigid, planar anchoring of the director and ideal conducting electrodes are assumed.

Direct numerical solution of the partial differential equations (7) by discretization in z and t appears feasible only in the D.C. case (no time dependence of $\mathbf{u}$) and has been done there [3, 13–15]. In general we either make a Fourier expansion in t [3], or expand the z dependence in an appropriate set of functions (the Galerkin method) [15, 16], or expand in both variables. Meaningful approximations are obtained by truncating the expansions, keeping one trial function for each relevant symmetry class (see §2) [3, 14–17]. In any case we obtain a relationship between $\sigma = \sigma' + i\sigma''$ and $\mathbf{q}$. The most dangerous mode is that with maximal growth rate $\sigma'_{\max}$ corresponding to some $\mathbf{q} = \mathbf{q}_{\max}$. The calculation gives $\sigma'_{\max}$ and $\mathbf{q}_{\max}$ (up to degeneracies) as a function of the external control parameter.

The basic state is stable when $\sigma'_{\max} < 0$, and the threshold for instability is obtained when $\sigma'_{\max}$ goes through zero. This condition leads to a determination of the critical voltage V_c (threshold) and critical wavenumber $\mathbf{q}_c$ as a function of the other parameters. Alternatively, we may determine the neutral surface $V_0(\mathbf{q})$ from the condition $\sigma'(\mathbf{q}) = 0$ (by taking the largest solution branch) and obtain V_c and $\mathbf{q}_c$ from minimization of $V_0(\mathbf{q})$. In the simplest case the instability is expected to lead to a state that is characterized by the linear mode with wavenumber $\mathbf{q}_c$. Therefore, if $\sigma'' = 0$ at threshold (stationary bifurcation) the structure is stationary, and if $\sigma'' \neq 0$ (Hopf bifurcation) a travelling pattern is expected, or maybe an oscillatory standing pattern.

In the §2 some symmetry considerations, which are essential in order to classify the modes, and some scaling properties are given. In §3 we present an explicit treatment of the D.C. case by trial functions, which exhibits some of the symmetry considerations and shows that our treatment includes the simpler instabilities as special cases (details are deferred to the Appendix). In §4 results for the A.C. and the D.C. cases are given, and in §5 the question of the determination of the amplitude of the structure slightly above threshold is addressed. Moreover, some problems of more-complicated patterns, and defects in this weakly non-linear region are discussed. We end by discussing some open problems.

2. Basic symmetries and scaling

It is useful to consider some symmetry properties of the boundary value problem (see equations (7) and (8)) [16]. We first consider the case without flexoelectric effect ($e_1 = e_3 = 0$). There are then two separate symmetries

$$V \to -V, \qquad (\phi, \theta, \psi, v_x, v_y, v_z) \to \pm(-\phi, \theta, \psi, v_x, v_y, v_z), \tag{9}$$

$$z \to -z, \qquad (\phi, \theta, \psi, v_x, v_y, v_z) \to \pm(\phi, \theta, -\psi, -v_x, -v_y, v_z). \tag{10}$$

The fact that the overall sign of $\mathbf{u}$ can be changed is simply a consequence of the linearity of equations (7) and (8). The symmetry (9) expresses the fact that without the flexoeffect the polarity of $\mathbf{E}$ does not affect $\hat{\mathbf{n}}$ and $\mathbf{v}$. The symmetry (10) is then a consequence of the overall reflection symmetry. From (10) it follows that there are two classes of solutions with

$$\begin{aligned}&(\phi(-z), \theta(-z), \psi(-z), v_x(-z), v_y(-z), v_z(-z))\\ &= \pm(\phi(z), \theta(z), -\psi(z), -v_x(z), -v_y(z), v_z(z)),\end{aligned} \tag{11}$$

where (+ denotes type I and − denotes type II). The lowest threshold is always obtained with a solution of type I. In the important, but special, case of a pure A.C. voltage, i.e. a time-periodic voltage with

$$V(t + T/2) = -V(t) \tag{12}$$

($T = 2\pi/\omega$ is the period), the symmetry (9) is evoked by the transformation $t \to t + T/2$. Thus the T-periodic solutions of equation (7) fall into two further classes with

$$(\phi(t + T/2), \theta(t + T/2), \psi(t + T/2), \mathbf{v}(t + T/2)) = \pm(-\phi(t), \theta(t), \psi(t), \mathbf{v}(t)), \tag{13}$$

where (+ denotes type A and − denotes type B). Usually the type A solution leads to the lowest threshold in the low frequency, conduction regime whereas the type B solution leads to the lowest threshold in the higher frequency, dielectric regime. For square wave A.C. excitation it is easy to see that in the limit $\omega \to 0$ the threshold for both modes tends to the D.C. threshold. For other waveforms (e.g. sinusoidal) this result presumably remains true in some approximation (see Appendix B of [3]).

With the flexoelectric effect the separate symmetries (9) and (10) are destroyed, but the combined symmetry $z \to -z$, $V \to -V$ remains (overall reflection). Thus for D.C. or combined D.C.–A.C. excitation where V has a definite polarity, the modes have no symmetry. As a consequence the motion of the fluid particles is helical in the oblique-roll regime [13–15]. However, in the pure A.C. case with (12) there are still two separate modes. The conduction mode consists of a superposition of a type IA and a type IIB function, and the dielectric mode is made up of a type IB and a type IIA part. In that case the motion of fluid particles is rather complicated and a net helical motion in oblique rolls does not appear to exist.

An important property of the boundary value problem (7), (8) is that if all lengths are measured in units of the layer thickness d, times in units of a typical director relaxation time $\tau_d \approx \alpha_0 d^2/\pi^2 k_0$ (k_0, α_0 are a typical elastic constant and viscosity, respectively) and uses the applied voltage (not the electric field), then τ_d enters only in the combination τ_d/τ_0, where $\tau_0 \approx \varepsilon\varepsilon_0/\sigma_0$ is a typical charge relaxation time (σ_0 is a typical conductivity). As a consequence the conductivity and thickness, which are varied quite easily in experiments, enter only in the combination $\sigma_0 d^2$. In the D.C. case $\sigma_0 d^2$ does not enter at all (see §3), so the threshold behaviour is independent of σ_0 and d ($q_c \approx d^{-1}$). This remains true in the lowest order, time Fourier approximation of the A.C. case, which is essentially valid in the conduction regime for $\tau_d \gg \tau_0$ [3, 17]. In the dielectric regime an analogous approximation gives $V_c \approx (k_0/\varepsilon_0)^{1/2} q_c d$ and $q_c d \approx (\tau_d \omega)^{1/2}$.

3. D.C. threshold

In the D.C. case the trial function approach leads to formulae for the threshold that can still be evaluated essentially analytically, and some generalization to the A.C. case is possible. We choose

$$(\phi, \theta, \psi, v_x, v_y) = (\phi^s, \theta^s, \psi^s, v_x^s, v_y^s) f_1(z) + (\phi^a, \theta^a, \psi^a, v_x^a, v_y^a) f_2(z), \tag{14}$$

$$v_z = v_z^s f_3(z) + v_z^a f_4(z), \tag{15}$$

where f_1 and f_3 are symmetric and f_2 and f_4 are antisymmetric in z, with $f_i = 0$, $i = 1, \ldots, 4$, and $\partial_z f_3 = \partial_z f_4 = 0$ at $z = \pm d/2$. A convenient choice is given in the

Appendix, and others are presented elsewhere [14, 15]. For a stationary bifurcation there is no time dependence at threshold, so we have only to deal with the right-hand side of equation (7). Projecting each component of equation (7) onto f_1 and f_2, or f_3 and f_4, respectively, we obtain a 12×12 system of algebraic equations. It is then feasible to eliminate successively v_x^s, v_x^a, ϕ^s, ϕ^a, v_y^a, v_y^s, v_z^s and v_z^a. The remaining 4×4 system can be written as

$$\mathbf{A}\mathbf{r} = \mathbf{0}, \qquad \mathbf{r} = (\theta^s, \psi^a, \theta^a, \psi^s), \tag{16}$$

$$\mathbf{A} = \begin{pmatrix} a_{11} + R^2 b_{11} & \underline{a_{12}} & \underline{Ra_{13}} & Ra_{14} \\ \underline{a_{21}} + R^2 \underline{b_{21}} & a_{22} & Ra_{23} & \underline{Ra_{24}} \\ \underline{Ra_{31}} & Ra_{32} & a_{33} + R^2 b_{33} & \underline{a_{34}} \\ Ra_{41} & \underline{Ra_{42}} & \underline{a_{43}} + R^2 \underline{b_{43}} & a_{44} \end{pmatrix}, \tag{17}$$

where $R = V\varepsilon_0^{1/2}/\pi$. The expressions for the coefficients a_{ij} and b_{ij} are given in the Appendix. Assuming a stationary bifurcation the condition that a mode with wavevector $\mathbf{q}$ is neutral is determined by the solvability condition of equation (16), $\mathrm{Det}(\mathbf{A}) = 0$. This is easily seen to lead to a cubic equation for $R^2 = R_0^2(\mathbf{q})$ which may be solved on a small computer and minimized with respect to $\mathbf{q}$.

Actually it is now easy, to derive various known special cases and additional simplifications from equations (16) and (17).

(*a*) No flexoelectric effect ($e_1 = e_3 = 0$). Then all the coefficients in $\mathbf{A}$ proportional to R vanish. The solvability condition reduces to the product of two first order equations for R^2 corresponding to type I and type II solutions. The neutral surface is determined by

$$R_0^2 = (a_{11}a_{22} - a_{12}a_{21})/(a_{12}b_{21} - b_{11}a_{22}), \tag{18}$$

(existence of non-trivial type I solutions) which is equivalent to that given previously [3, 17]. Equation (18) is easily extended to the A.C. case (conduction range) in the lowest order, time Fourier expansion [3, 17].

(*b*) Generalized one dimensional model. Then all of the z dependence is neglected so that most of the integrals in the Appendix are zero (only M_4 and M_6 are non-zero). As a consequence all the terms in equation (17) that are underlined vanish. Again there are two first order equations in R^2. The neutral surface is then

$$R_0^2 = a_{11}a_{44}/(a_{14}a_{41} - b_{11}a_{44}), \tag{19}$$

which is equivalent to the previous result by Madhusudana *et al.* [19]. In that paper the influence of the flexoelectric effect on oblique rolls was analysed for the first time.

(*c*) Normal rolls. For $p = 0$ many coefficients in $\mathbf{A}$ vanish and the condition

$$(a_{11} + R^2 b_{11})(a_{33} + R^2 b_{33}) - R^2 a_{13}a_{31} = 0 \tag{20}$$

is obtained. Even when the terms proportional to p^2 are included the solvability condition remains quadratic in R^2. This is all we need to determine the continuous transition to oblique rolls. Without the flexoeffect $a_{13}a_{31} = 0$ and equation (20) simplifies further.

(*d*) Longitudinal rolls. For $q = 0$, $a_{13} = a_{31} = a_{24} = a_{42} = b_{21} = b_{43} = 0$. Then the flexocoefficients only appear in the combination $e_1 - e_3$ and the solvability condition, which is quadratic in R^2, gives the static instability first considered by Bobylev

and Pikin [20]. Without the flexoelectric effect the condition reduces to

$$R_0^2 \varepsilon_a = k_{11} M_1 + k_{22} p^2 + h_x^2 - h_z^2 - \frac{p^2 (k_{11} - k_{22})^2 M_3^2}{k_{11} p^2 + k_{22} M_2 + h_y^2 - h_z^2}, \qquad (21)$$

which is also obtained from equation (18) with $q = 0$. (h_x, h_y and h_z describe an additional magnetic field along one of the axes; see Appendix.) This relationship describes the periodic splay-twist Fréedericksz transition discovered by Lonberg and Meyer for materials with large k_{11}/k_{22} [21].

4. Results of the linear theory

Some rigorous results on the threshold behaviour in the D.C. case including the flexoelectric effect were given before [13, 14]. Here we wish to add some results. In figure 1 the angle of the rolls with respect to the molecular alignment, α, as a function of the flexoelectric strength is plotted (otherwise standard parameters of MBBA, see [14]). Setting $e_1 + e_3 = 0$ and varying $e_1 - e_3$ leads to a rather steep transition from normal rolls with $\alpha = 0$ ($e_1 - e_3 < 0{\cdot}7 \times 10^{-4}$ esu) to parallel rolls with $\alpha = 90°$ ($e_1 - e_3 > 3{\cdot}2 \times 10^{-4}$ esu). The latter case corresponds to the non-convective Bobylev–Pikin transition [20]. Note that the results are invariant under a sign change of e_1 and e_3. In the other extreme, $e_1 - e_3 = 0$, the oblique rolls always remain below a limiting angle. Also shown in figure 1 is the case $e_1 + e_3 = -7{\cdot}0 \times 10^{-4}$ esu, which corresponds to a recent measurement for MBBA [22]. The point $e_1 - e_3 = 1{\cdot}2 \times 10^{-4}$ esu where $\alpha = 43{\cdot}6°$ corresponds to a measurement of this quantity [23]. Also plotted is the curve according to the approximate treatment of §3.

In figure 2 we show α as a function of the anisotropy of the conductivity $\sigma_\parallel/\sigma_\perp$ for flexocoefficients ξe_1 and ξe_3 with $e_1 = -2{\cdot}9 \times 10^{-4}$ esu and $e_3 = -4{\cdot}1 \times 10^{-4}$ esu from [22, 23] and $0 \leqslant \xi \leqslant 1$ (otherwise standard MBBA parameters). Without the flexoelectric effect ($\xi = 0$) the normal–oblique transition (Lifshitz point) occurs at $\sigma_\parallel/\sigma_\perp = 1{\cdot}76$ [3]. Turning on the flexoelectric effect moves the Lifshitz point to the left until the roll angle remains finite for all $\sigma_\parallel/\sigma_\perp > 1$. For $\xi = 1$ the roll angle is rather insensitive to changes of $\sigma_\parallel/\sigma_\perp$ but the threshold diverges for $\sigma_\parallel/\sigma_\perp \to 1$, as is the case for all values of $\xi < 1$. The broken curves show the results of the approximate treatment for $\xi = 0$, $0{\cdot}2$ and 1.

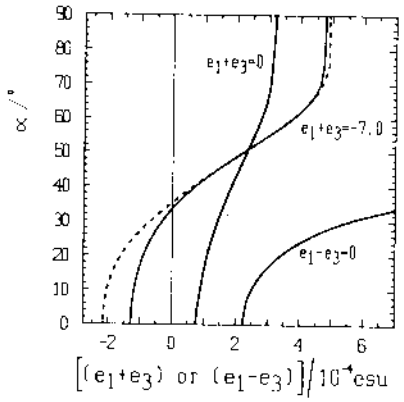

Figure 1. Roll angle α with respect to the molecular alignment as a function of $e_1 + e_3$ or $e_1 - e_3$, the other quantity being constant, calculated using MBBA parameters ($\sigma_\parallel/\sigma_\perp = 1{\cdot}5$).

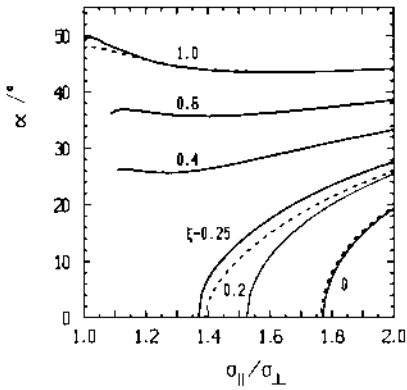

Figure 2. Roll angle α as a function of the anisotropy of the conductivity $\sigma_\parallel/\sigma_\perp$ for various values of the flexoelectric strength ξ: the flexocoefficients are ξe_1 and ξe_3.

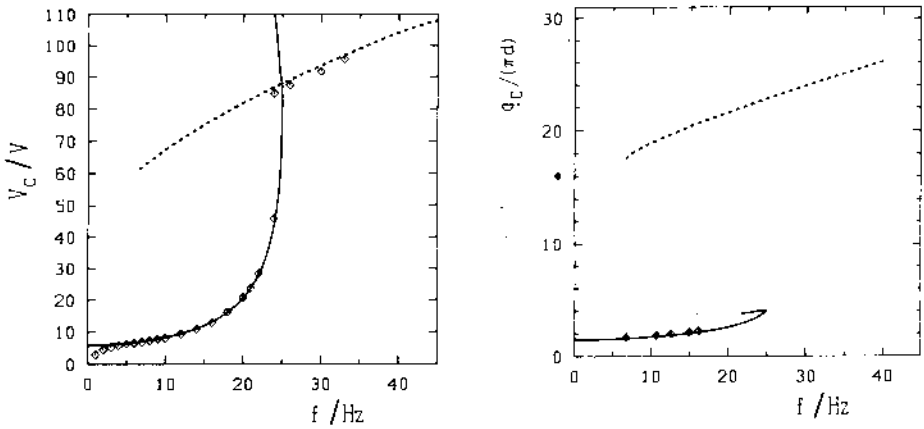

Figure 3. Threshold voltage, V_c, and wavenumber q_c in units π/d as a function of frequency for MBBA with $\sigma_\perp d^2 = 0{\cdot}28 \times 10^{-4}\Omega^{-1}\,\mathrm{m}^{-1}\,\mu\mathrm{m}^2$, $\sigma_\parallel/\sigma_\perp = 1{\cdot}65$ and reduced flexocoefficients (see text).

Increasing ξ beyond unity leads to a finite threshold at $\sigma_\parallel/\sigma_\perp = 1$, and even for negative anisotropy of the conductivity $\sigma_\parallel - \sigma_\perp$. Then the Carr–Helfrich mechanism, which is ordinarily the main driving force for the instability, becomes unimportant and the instability becomes purely driven by the flexoeffect. This type of effect was also found by Madhusudana and Ragunathan [24] within a one dimensional model at finite frequency and is discussed there.

Now turning to the A.C. case we first show in figure 3 a comparison of the theoretical results for MBBA with experiments by Kai [25] on a rather thick ($d = 100\,\mu\mathrm{m}$) and clean sample. $\sigma_\perp$ was not measured and we chose $0{\cdot}28 \times 10^{-8}\Omega^{-1}\,\mathrm{m}^{-1}$ to fit the cut-off frequency with $\sigma_\parallel/\sigma_\perp = 1{\cdot}65$. The flexocoefficients were chosen as $e_1 = -1{\cdot}1 \times 10^{-4}$ esu and $e_3 = -2{\cdot}0 \times 10^{-4}$ esu, which is considerably smaller than the values derived from [22, 23]. For the measured values we would obtain oblique rolls at threshold of the dielectric regime which is in agreement with previous calculations using the one dimensional model [24]. However, normal rolls are observed at threshold [25] (the well known chevrons are connected with a secondary instability, see §6. Since it is well known that measurements of the

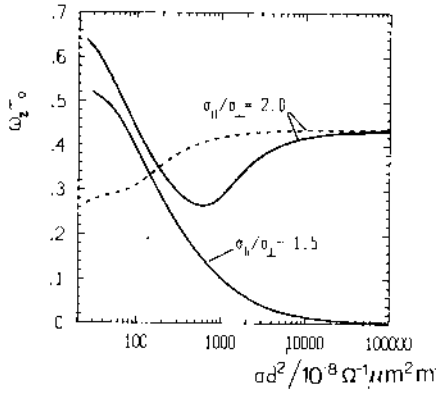

Figure 4. Reduced Lifshitz point frequency $\omega_c\tau_0$ as a function of $\sigma_\perp d^2$ in units $10^{-8}\Omega^{-1}\,m^{-1}\,\mu m^2$ for MBBA and two values of $\sigma_\parallel/\sigma_\perp$ (——) with and (– – –) without the flexoeffect.

e_j are problematic, we suggest that their values are in fact considerably lower than suggested by the results of [22, 23] (for example we mention the result of $e_1 + e_3 = -3{\cdot}1 \times 10^{-4}$esu found in [26] instead of $-7{\cdot}0 \times 10^{-4}$esu in [22]).

The agreement of the frequency-dependent threshold and the wavenumber with experiment is seen to be good (the wavenumber in the dielectric regime was not measured), except at frequencies, f, below about 4 Hz. Here, presumably, electrochemical effects become important. For thinner or cleaner samples ($\sigma_0 d^2$ smaller) the cut-off frequency in units of τ_0^{-1} becomes smaller and the threshold as well as the reduced wavenumber qd in the dielectric regime are decreased [15, 16, 24], behaving approximately as $(\sigma_0 d^2)^{1/2}$ (see §2).

In figure 4 the Lifshitz point frequency ω_c multiplied by $\tau_0 = \varepsilon_0\varepsilon_\perp/\sigma_\perp$ is plotted as a function of $\sigma_\perp d^2$ for $\sigma_\parallel/\sigma_\perp = 1{\cdot}5$ and $\sigma_\parallel/\sigma_\perp = 2{\cdot}0$ (otherwise MBBA parameters). Without the flexoeffect there are normal rolls everywhere for $\sigma_\parallel/\sigma_\perp$ of 1·5 [3]. For $\sigma_\parallel/\sigma_\perp$ equal to 2·0 there is a plateau value for $\omega_c\tau_0$ at large values of σd^2 and a moderate decrease of $\omega_c\tau_0$ when σd^2 is decreased [3]. The plateau value is obtained by the lowest order, time Fourier expansion. With the flexoeffect (coefficients from [22, 23]) we always have an oblique-roll regime at low frequencies. For $\sigma_\parallel/\sigma_\perp = 1{\cdot}5$, however, $\omega_c\tau_0 \to 0$ for $\sigma d^2 \to \infty$, whereas $\omega_c\tau_0$ is non-monotonic for $\sigma_\parallel/\sigma_\perp = 2{\cdot}0$. Obviously for large values of σd^2 the influence of the flexoeffect becomes small, which can be understood from the fact that it drops out of the lowest order, time Fourier approximation, which then becomes valid. As far as we can see these effects cannot be captured in a one dimensional model.

5. Weakly non-linear region

In the vicinity of the threshold of EHC the spatially periodic solutions and their slow space and time modulations can be described by equations for a complex amplitude (or envelope) A, the so-called amplitude (or envelope) equations [3, 27, 28]. The physical quantities $\mathbf{u} = (\phi, \theta, \psi, \mathbf{v})$ are then obtained in the form

$$u_j = \varepsilon^{1/2}\,[A(X, Y, T)\,U_j \exp[\mathrm{i}(q_c x + p_c y)] + \text{c.c.}]\,w_j(z, t) + O(\varepsilon), \qquad (22)$$

($|U_j| = 1$) where $\varepsilon = (V^2 - V_c^2)/V_c^2$ measures in a dimensionless way the distance from threshold,

$$X = \varepsilon^{1/2}x, \qquad Y = \varepsilon^{1/2}y, \qquad T = \varepsilon t \qquad (23)$$

are slow space and time variables, and c.c. denotes the complex conjugate. The w_j correspond to the linear modes discussed before.

The slow variables capture the shape of the neutral surface, which is parabolic in q and p around $\mathbf{q}_c = (q_c, p_c)$, and the behaviour of the linear growth rate. Near the Lifshitz point, where the curvature of the neutral surface with respect to p vanishes, a different scaling for the Y coordinate has to be used [3, 27, 28]. This case is not considered here.

Carrying the expansion of the equations up to order $\varepsilon^{3/2}$ we obtain as a solvability condition the envelope equation

$$T_0 \partial_T A = [\xi_1^2 \partial_X^2 + \xi_2^2 \partial_Y^2 + 2\xi_1 \xi_2 a \partial_X \partial_Y + 1 - |A|^2]A, \tag{24}$$

as well as the normalization of the w_j in equation (22). In the normal roll case $a = 0$ and in general $0 \leqslant a < 1$. The parameters in equation (24) are calculated from the linear analysis [3, 27, 28]. Results for MBBA within the lowest order, time Fourier expansion in the conduction regime are given elsewhere for normal [3, 29] and for oblique [30] rolls. In an experiment by Rasenat *et al.* [31] the angle θ of the director was measured near threshold in the normal roll regime by an elaborate optical method. Good agreement with the linear modes and the $\varepsilon^{1/2}$ law, including the calculated normalization, was found for $\varepsilon \approx 0{\cdot}1$.

By rotation and scaling of the coordinate system equation (24) can be transformed into the more symmetric form [32]

$$\partial_{T'} A = (\nabla + 1 - |A|^2)A, \quad \nabla = \partial_{X'}^2 + \partial_{Y'}^2. \tag{25}$$

Equation (25) has stationary solutions of the form

$$A = (1 - Q^2 - P^2)^{1/2} \exp[\mathrm{i}(QX' + PY')]. \tag{26}$$

From equation (22) we see that they describe roll patterns above threshold with the wavevector

$$\mathbf{q} = [q_c + \varepsilon^{1/2}(Q \cos\alpha/\xi_+ - P \sin\alpha/\xi_-), \; p_c + \varepsilon^{1/2}(Q \sin\alpha/\xi_+ + P \cos\alpha/\xi_-)], \tag{27}$$

where

$$\xi_\pm^2 = \tfrac{1}{2}\{\xi_1^2 + \xi_2^2 + [(\xi_1^2 - \xi_2^2)^2 + 4a^2 \xi_1^2 \xi_2^2]^{1/2}\}, \quad \tan(2\alpha) = 2a\,\xi_1 \xi_2/(\xi_1^2 - \xi_2^2).$$

A linear stability analysis of the solution (26) shows that it is linearly stable for $Q^2 + P^2 < 1/3$ [27]. This is a direct generalization of the Eckhaus instability criterion for quasi-one dimensional systems [33, 34]. We see that there is a stable two dimensional wavevector band inside the range of existence $Q^2 + P^2 < 1$. Thus, even in the normal roll range under ideal conditions where the effect of fluctuations and inhomogeneities, including boundaries, are negligible, oblique patterns should be experimentally accessible.

If the system is initialized in the unstable region the pattern evolves to the bandcentre and ends up with a final state which is expected to be $\mathbf{Q} = \mathbf{K}$. $\mathbf{K}$ is the modulation wavevector of the most rapidly growing disturbance. This evolution process was studied in the one dimensional limit theoretically [35] and experimentally for EHC [36]. In the two dimensional case the roll system is first modulated by the unstable mode, which then tends to evolve into dislocations which are created in pairs.

By motion and destruction of these defects the system changes the wavevector of the pattern and again ends up near $\mathbf{Q} - \mathbf{K}$. In the presence of lateral boundaries this process is triggered at the boundaries [37].

States with $\mathbf{Q} \neq \mathbf{0}$ in the Eckhaus stable range are metastable. Evolution to the bandcentre can occur by the motion of dislocations that are nucleated by finite fluctuations or perturbations [32]. Such a dislocation is described by a simple zero of the complex field A. When going around the zero the phase of A changes by $\pm 2\pi$. Equation (25) can be used to describe the structure and dynamics of dislocations as well as some nucleation properties. Stationary dislocations exist only at the bandcentre $\mathbf{Q} = \mathbf{0}$. Away from the bandcentre ($\mathbf{Q} \neq \mathbf{0}$) the direction of motion is perpendicular to the displacement wavevector $\mathbf{Q}$ (this is also true in physical units).

The motion of dislocations can be separated into motion along the roll axis (climb) and perpendicular to it (glide). Whereas the climb changes the spacing of the rolls, the glide changes the orientation of the roll pattern. In isotropic systems, glide is only possible for non-potential situations [38]. In our analysis climb and glide motion are equivalent. This is true as long as non-adiabatic effects which couple the slow and fast variations can be neglected. Due to such effects the defects will have preferred positions in the underlying pattern as far as the glide is concerned. Therefore, gliding of dislocations will not quite act as an ideal selection mechanism, in contrast to climb, and leaves a wavenumber band with respect to orientation. Near to threshold such effects are expected to be small.

Another difference from isotropic systems concerns the velocity of isolated dislocations. Whereas for isotropic systems the velocity V scales essentially as $Q^{3/2}$, for anisotropic systems like EHC the velocity V is essentially proportional to Q (from now on we choose $P = 0$). A detailed analysis of equation (25) [32] gives, in the limit $|Q| \ll 1$,

$$\left.\begin{aligned} |V| &= \mu |Q|, \\ \mu &= \begin{cases} 2/\ln(R/1{\cdot}13), & \text{for } |V| R \ll 1, \\ 2/\ln(3{\cdot}29/|V|), & \text{for } |V| R \gg 1, \end{cases} \end{aligned}\right\} \tag{28}$$

where $R = (X'^2 + Y'^2)^{1/2} \gg 1$ is the system size in scaled units. By numerical simulation we have obtained the velocity in the full Q range and so have tested the validity of equation (28). A pseudo-spectral method with periodic boundary condition was used [39]. Two dislocations with opposite sign were initiated in a cell, which was sufficiently large that the influence of dislocation pairs in the neighbouring cells could be neglected initially. In figure 5 the velocity versus time behaviour of the motion of one of the dislocations in the simulations is shown for $Q = 0{\cdot}125$. After an initial transient the dislocation moves with nearly constant velocity. The slight slope of the curve is due to the interaction with the other dislocations in the periodic grid. When the dislocations come near to the cell boundary the interaction with the dislocation of opposite sign in the next cell becomes strong. Thus the velocity increases until the defect annihilates. A similar behaviour of the annihilation process at the boundary was seen in experiment [40]. In figure 6 the numerical results (circles) for the velocity in the plateau region are plotted against Q. The solid curve gives the analytic result for $VR \gg 1$ from equation (29). Clearly the analysis remains quite good even for moderate values of Q. For comparison with experiment the quantities

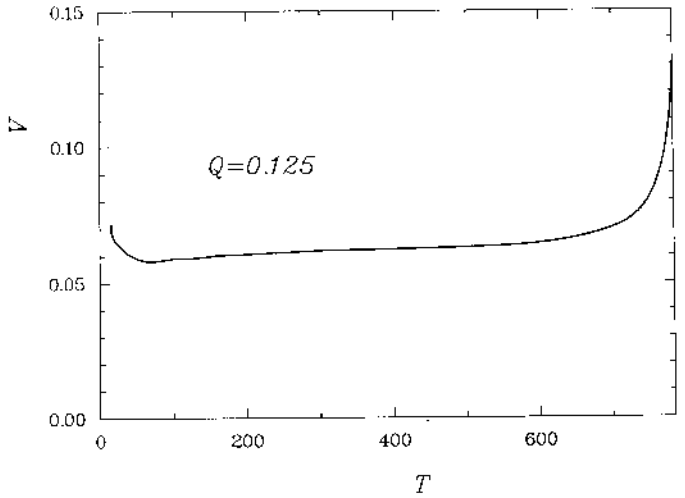

Figure 5. Velocity, V, of a dislocation versus time T in reduced units (see text). The defect was initiated at $T = 0$ and annihilates at time $T \approx 800$ at the cell boundary.

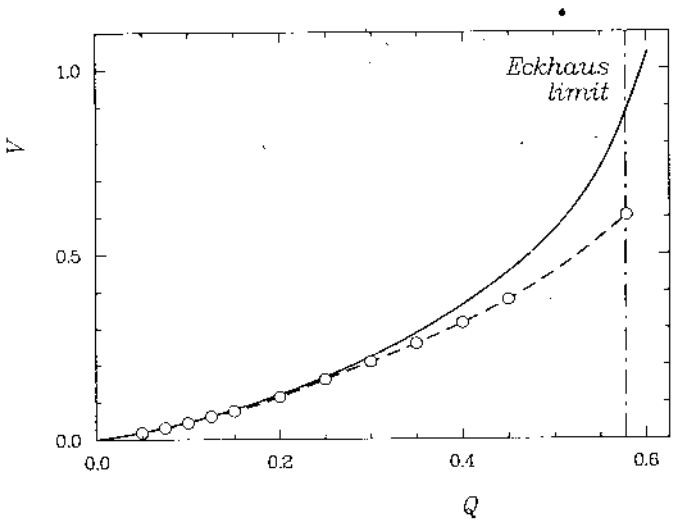

Figure 6. Velocity, V, of an isolated defect versus wavenumber displacement Q. (○) Numerical results and (——) the analysis.

Q and V have to be transformed into physical units. The detailed rescaling is given in [32].

In the oblique roll region line defects connecting roll patterns with $p > 0$ and $p < 0$ are also observed [7, 8, 41]. These grain boundaries can be studied in the weakly non-linear region using two coupled amplitude equations

$$\left.\begin{aligned} T_0\partial_T A &= [\xi_1^2\partial_X^2 + \xi_1^2\partial_Y^2 + 2\xi_1\xi_2 a\partial_X\partial_Y + 1 - |A|^2 - \gamma|B|^2]A, \\ T_0\partial_T B &= [\xi_1^2\partial_X^2 + \xi_1^2\partial_Y^2 - 2\xi_1\xi_2 a\partial_X\partial_Y + 1 - |B|^2 - \gamma|A|^2]B, \end{aligned}\right\} \tag{29}$$

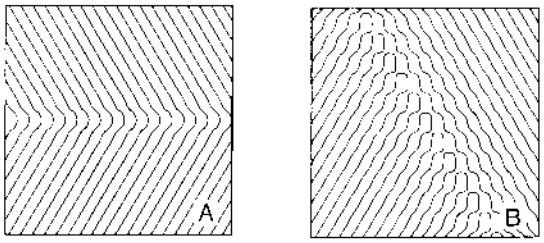

Figure 7. Node lines of u for grain boundaries between regions with p and $-p$ according to equations (29) and (30) for $a = 0{\cdot}2$, $\xi_1 = 0{\cdot}3$, $\xi_2 = 0{\cdot}06$, $\gamma = 1{\cdot}005$, $p_c/q_c = 0{\cdot}6$, $\varepsilon = 0{\cdot}1$. (*a*) The usual zig-zag boundary in the x direction. (*b*) The non-adiabatic grain boundary parallel to one of the roll systems.

which can also be obtained from weakly non-linear perturbation analysis. A typical physical field u can then be written as

$$u_j \approx \varepsilon^{1/2} \{A(X, Y, T)\exp[\mathrm{i}(q_c x + p_c y)] + B(X, Y, T) \times \exp[\mathrm{i}(q_c x - p_c y)] + \text{c.c.}\} + O(\varepsilon). \tag{30}$$

The slow variables X, Y and T are scaled as in equation (23). For $0 < \gamma \leqslant 1$ equations (29) exhibit stable bimodal solutions (rectangles) whereas for $\gamma > 1$ stable roll solutions exist, which is usually the case for EHC. γ has not been calculated. We want to study solutions at the bandcentre $(q_c, \pm p_c)$ where the amplitudes A and B are real functions. Numerical simulations show that equation (29) has grain boundary solutions with the boundary in any direction in space. The solution with the grain boundary parallel to the x direction (zig-zag structure, figure 7(*a*)) has the lowest free energy. This is in agreement with experiment where mostly this type of zig-zag structure is observed. Another interesting direction of the domain wall (see figure 7(*b*)) is parallel to one of the roll systems. Although it has a higher free energy it is sometimes observed in experiments [41]. This stabilization is presumable due to non-adiabatic effects that are not included in the envelope approximation. We have used parameters typical for MBBA-like materials in the oblique roll range [3]. In order to obtain the strong modulation of the structure, seen in some experiments [7, 8], we have to be near to the point where roll solutions cross over to rectangles ($\gamma = 1$) (for increasing γ the modulation length decreases). This means that in these experiments we have to be near to the rectangular state. It would be interesting to find a material where the bimodal structure already occurs at threshold.

6. Concluding remarks

We have given an overview of recent theoretical results for the threshold and near-threshold behaviour of EHC within the standard theory where the electrical properties of the planarly aligned nematic are described by (anisotropic) ohmic conductance, linear polarizability and flexoelectricity. All of these effects have an important influence on EHC.

At this time we can understand qualitatively almost all of the effects which are observed at threshold. In many cases quantitative agreement is achieved. A very interesting exception is the extended travelling roll patterns, normal or oblique which

are sometimes observed in fairly thin ($d < 50\,\mu$m) samples (MBBA or similar materials) of intermediate conductivity [4, 6, 42], which have been identified to be connected with a primary (forward) Hopf bifurcation [6]. The effect occurs most often in the conduction regime near the cut-off frequency. Unfortunately, in this region the system is also quite susceptible to inhomogeneities. Thus, the persistent spatially localized travelling patterns which are sometimes observed are presumably in most cases, if not always, due to imperfections.

The standard theory does not appear to give a primary Hopf bifurcation for MBBA-like materials ($\varepsilon_a < 0$) under D.C. or simple A.C. driving. There appear to be two promising directions in which the theory could be extended: according to the discussion in §2 there are two rather complicated but nevertheless independent modes that correspond to the conduction and the dielectric instability mechanisms, as long as the sample is up–down symmetric and there is sinusoidal-like A.C. driving (symmetry (12)). Coupling of two (stationary) modes is known to lead easily to a Hopf bifurcation. Unfortunately, since the critical wavenumbers are quite different, the coupling has apparently to be fairly strong. Evidence that this type of mechanism can work is provided by the fact that with a non-sinusoidal driving that violates equation (12) we can produce a Hopf bifurcation. Maybe a disturbance of the up–down symmetry is present in some samples, possibly involving tilt at the boundary.

On the other hand, it may be necessary to introduce an additional dynamic process that is not included in the standard theory. Here electrochemical processes, especially those connected with charge-transfer at the electrodes, are the most likely candidates.

In either case it now appears important to characterize experimentally the samples that show travelling waves in greater detail. Asymmetries and electrochemical effects probably both show up in the frequency-dependent I–V characteristics below threshold and could be investigated there. In this context it appears useful to point out the necessity of establishing a new standard material with $\varepsilon_a < 0$. It should be electrochemically stable and all of the material parameters have to be measured accurately.

Concerning the behaviour above, but still near to threshold (weakly non-linear region) there are several unexplained effects. First the undulated roll solutions, whose existence in a range between the normal and the oblique roll regimes near the Lifshitz point seems well established [7, 8], pose a problem. The universal amplitude theory of the type discussed in §5 and valid in the vicinity of the Lifshitz point [3, 27, 28] does not allow the continuous transition from normal to undulated rolls which is apparently observed. Although it is possible to incorporate such a transition in a phenomenological description, it does not appear to be possible to remedy the situation in the theory by carrying the amplitude expansion to higher order in the standard way, as can be seen by using a phase diffusion approach that is more generally valid [43].

It appears likely however that inclusion of so-called mean flow effects which account for an additional slow and weakly damped mode which is excited by spatial variations of the amplitude function, introduced in §5, will alter the situation. Such effects are well known for isotropic systems [44] and were recently calculated for EHC using simplifying stress free boundary conditions at the upper and lower plates. Here they destabilize all roll solutions at threshold by an undulatory instability [30]. The undulations are, however, not stabilized. Instead they appear to render the system weakly turbulent. There is reasonable hope that with realistic boundary conditions this instability is weakened. Then undulations might stabilize in some range and a continuous transition between normal and undulated rolls may become possible.

There is also reasonable hope that the direct transition to turbulence is not totally abolished by realistic boundaries but only transformed into a secondary transition occurring at a slightly higher threshold, as is observed [4–6]. This secondary transition involving irregular motion of dislocations is seen not only for stationary and travelling rolls in the conduction regime, but presumably also the transition to chevrons in the dielectric regime is of this general nature. One then also observes the spontaneous appearance of defects, which, as their density grows above threshold, gradually order along lines which form the boundaries of the chevron domains.

Finally, we point out that even in the stable region the motion of defects must be expected to be influenced by mean-flow effects as is known from isotropic systems [45].

Work towards an understanding of some of these fascinating phenomena is in progress. Of course, even more challenges are provided by the rich behaviour found further away from threshold.

We thank I. Rehberg and M. de la Torre for many discussions and exhibitions of real experiments. Stimulating discussions with A. Joets, S. Kai, M. Kaiser, N. V. Madhusudana and R. Ribotta are gratefully acknowledged. This work was supported by Deutsche Forschungsgemeinschaft (Sonderforschungsbereich 212, Bayreuth), Fonds der chemischen Industrie, Emil-Warburg-Stiftung, Bayreuth, and HLRZ, Jülich.

Appendix

We measure lengths in units of d/π, normalize the functions f_1, f_2, f_3 and f_4 such that $\int_{\pi/2}^{\pi/2} f_i^2(z)\,dz = 1$, and define the following integrals (the integration range is always from $-\pi/2$ to $+\pi/2$):

$$\left.\begin{aligned}
M_1 &= -\int f_1 \partial_z^2 f_1\,dz, & M_2 &= -\int f_2 \partial_z^2 f_2\,dz,\\
M_3 &= \int f_1 \partial_z f_2\,dz, & M_4 &= \int f_1 f_3\,dz,\\
M_5 &= \int f_2 f_4\,dz, & M_6 &= \int f_2 \partial_z f_3\,dz,\\
M_7 &= \int f_1 \partial_z f_4\,dz, & M_8 &= -\int f_3 \partial_z^2 f_1\,dz,\\
M_9 &= -\int f_3 \partial_z^3 f_2\,dz, & M_{10} &= -\int f_3 \partial_z^2 f_3\,dz,\\
M_{11} &= -\int f_4 \partial_z^2 f_2\,dz, & M_{12} &= -\int f_4 \partial_z^3 f_1\,dz,\\
M_{13} &= -\int f_4 \partial_z^2 f_4. &&
\end{aligned}\right\} \quad \text{(A1)}$$

Next we define the quantities

$$\left.\begin{aligned}
H_{1,2} &= [(\varepsilon_\parallel q^2 + \varepsilon_\perp p^2)M_{4,5} + \varepsilon_\perp M_{8,11}]\sigma_a/\sigma_{1,2} - \varepsilon_a M_{4,5},\\
\sigma_{1,2} &= \sigma_\parallel q^2 + \sigma_\perp (p^2 + M_{1,2}),\\
V_{1,2} &= [\alpha_2 q^2 M_{4,5} \pm \alpha_3 M_3 (M_{6,7} + p^2\beta_{1,5}/\beta_{2,6})]/h_{1,2},\\
V_{3,4} &= [\alpha_3 M_{6,7} + (\alpha_3 p^2 - \alpha_2 q^2)\beta_{1,5}/\beta_{2,6}]/h_{1,2},\\
h_{1,2} &= \beta_{3,7} - p^2\beta_{4,8}\beta_{1,5}/\beta_{2,6},\\
\beta_{1,5} &= (\delta - \alpha_4 q^2/2 + \eta_2 M_{2,1})M_{6,7},\\
\beta_{2,6} &= \delta p^2 + \eta_1 q^4 + (\eta_2 p^2 + \alpha_4 q^2/2)M_{2,1},\\
\beta_{4,7} &= (\delta - \alpha_4 q^2/2)M_{6,7} + \eta_2 M_{9,12},\\
\beta_{3,7} &= (\alpha_4 p^2/2 + \eta_1 q^2)q^2 - \eta_2 M_{6,7} M_{9,12} - [(\eta_1 + \alpha_1 + \alpha_6)q^2\\
&\quad + \eta_2 p^2]M_{6,7}^2 - (\eta_2 - \alpha_3 - \alpha_4)q^2 M_{10,13},\\
\delta &= (\eta_1 + \eta_2 + \alpha_1)q^2 + \eta_2 p^2,\\
\eta_1 &= (\alpha_4 + \alpha_5 - \alpha_2)/2, \qquad \eta_2 = (\alpha_3 + \alpha_4 + \alpha_6)/2.
\end{aligned}\right\} \quad \text{(A2)}$$

The α_i are the Leslie viscosity coefficients.

Then we have

$$\left.\begin{aligned}
a_{11,33} &= k_{22}p^2 + k_{33}q^2 + h_x^2 - h_z^2 + k_{11}M_{1,2},\\
a_{22,44} &= k_{11}p^2 + k_{33}q^2 + h_x^2 - h_y^2 + k_{22}M_{2,1},\\
b_{11,33} &= \varepsilon_a(q^2\sigma_a/\sigma_{1,2} - 1) + q^2 V_{1,2}H_{1,2},\\
a_{12} &= a_{21} = -a_{34} = -a_{43} = -p(k_{11} - k_{22})M_3,\\
b_{21,43} &= -pq^2 V_{3,4}H_{1,2},\\
a_{13,31} &= \mp q^2(e_1 + e_3)(M_3\sigma_a/\sigma_{1,2} \pm V_{1,2}M_{6,7}),\\
a_{24,42} &= p^2q^2(e_1 + e_3)V_{3,4}M_{4,5},\\
a_{23,41} &= p[-(e_1 - e_3) + q^2(e_1 + e_3)(\sigma_a/\sigma_{1,2} + V_{3,4}M_{6,7})],\\
a_{14,32} &= -p[(e_1 - e_3) + q^2(e_1 + e_3)V_{1,2}M_{4,5}].
\end{aligned}\right\} \quad \text{(A3)}$$

The k_{ii} are the usual Frank elastic constants and h_x, h_y and h_z denotes a magnetic field along the respective axis in units $(\chi_a\mu_0)^{1/2}(d/\pi)$ (only one h_i may be non-zero). The physical wavenumbers are given by $q\pi/d$ and $p\pi/d$.

A useful set of trial functions is [14]

$$\left.\begin{aligned}
f_1 &= (30/\pi^5)^{1/2}(\pi^2/4 - z^2), \qquad f_2 = (840/\pi^7)^{1/2}(\pi^2/4 - z^2)z,\\
f_3 &= (630/\pi^9)^{1/2}(\pi^2/4 - z^2)^2, \qquad f_4 = (27\,720/\pi^{11})^{1/2}(\pi^2/4 - z^2)^2 z.
\end{aligned}\right\} \quad \text{(A4)}$$

Then we have

$$\begin{aligned}
M_1 &= 10/\pi^2, & M_2 &= 42/\pi^2,\\
M_3 &= (7/\pi^2)^{1/2}, & M_4 &= (27/28)^{1/2},\\
M_5 &= (11/12)^{1/2}, & M_6 &= -(12/\pi^2)^{1/2},
\end{aligned}$$

$$M_7 = [33/(7\pi^2)]^{1/2}, \qquad M_8 = (84/\pi^4)^{1/2}$$
$$M_9 = 3^{1/2}\,(84/\pi^3), \qquad M_{10} = 12/\pi^2,$$
$$M_{11} = 33^{1/2}\,(6/\pi^2), \qquad M_{12} = 0,$$
$$M_{13} = 44/\pi^2.$$

References

[1] Goossens, W. J. A., 1978, *Advances in Liquid Crystals*, edited by G. H. Brown, Vol. 3 (Academic Press), p. 1.

[2] Blinov, L. M., 1983, *Electro-optical and Magneto-optical Properties of Liquid Crystals* (Wiley).

[3] Bodenschatz, E., Zimmermann, W., and Kramer, L., 1988, *J. Phys., Paris*, **49**, 1875.

[4] Kai, S., and Hirakawa, K., 1978, *Suppl. Prog. theor. Phys.*, **64**, 212; 1977, *Mem. Fac. Engng Kyushu Univ.*, **36**, 269.

[5] Kai, S., 1987, *Noise in Nonlinear Dynamical Systems*, edited by P. V. E. McClintock and F. Moss (Cambridge University Press). Yamazaki, H., Kai, S., and Hirakawa, K., 1987, *J. phys. Soc. Japan*, **56**, 1.

[6] Rehberg, I., Rasenat, S., and Steinberg, V., 1989, *Phys. Rev. Lett.*, **62**, 756.

[7] Joets, A., and Ribotta, R., 1984, *Cellular Structures in Instabilities*, edited by J. E. Wesfreid and S. Zaleski (Springer-Verlag), p. 294. Ribotta, R., Joets, A., and Lin Lei, 1986, *Phys. Rev. Lett.*, **56**, 1595.

[8] Joets, A., and Ribotta, R., 1986, *J. Phys., Paris*, **47**, 595.

[9] Hohenberg, P. C. and Cross, M. C., 1987, *Fluctuations and Stochastic Phenomena in Condensed Matter Physics*, edited by L. Garrido (Springer-Verlag), p. 55.

[10] Wesfreid, J. E. (editor), 1988, *Propagation in Systems Far From Equilibrium* (Springer-Verlag). Güttinger, W., and Dangelmayr, G. (editors), 1987. *The Physics of Structure Formation* (Springer-Verlag).

[11] Meyer, R. B., 1969, *Phys. Rev. Lett.*, **22**, 918. Prost, J., and Marcerou, J. P., 1977, *J. Phys., Paris*, **38**, 315.

[12] de Gennes, P. G., 1974, *The Physics of Liquid Crystals* (Clarendon Press).

[13] Raghunathan, V. A., and Madhusudana, N. V., 1988, *Pramana J. Phys.*, **31**, L163.

[14] Thom, W., Zimmermann, W., and Kramer, L., 1989, *Liq. Crystals*, **4**, 309.

[15] Thom, W., 1988, Diploma Thesis, Bayreuth.

[16] Zimmermann, W., and Thom, W. (to be published).

[17] Zimmermann, W., and Kramer, L., 1985, *Phys. Rev. Lett.*, **55**, 402.

[18] Zimmermann, W., 1987, Ph.D. thesis, Universität Bayreuth.

[19] Madhusudana, N. V., Raghunathan, V. A., and Sumathy, K. R., 1987, *Pramana J. Phys.*, **28**, L311; there are some misprints in equations (5) and (7).

[20] Bobylev, Yu., and Pikin, S. A., 1977, *Zh. eksp. teor. Fiz.*, **72**, 369 (*Soviet Phys. JETP*, **45**, 195 (1977).) Barnik, M. I., Blinov, L. M., Trufanov, A. N., and Umanskii, B. A., 1977, *Zh. eksp. teor. Fiz.*, **73**, 1936 (1977, *Soviet Phys. JETP*, **46**, 1016).

[21] Lonberg, F., and Meyer, R. B., 1985, *Phys. Rev. Lett.*, **55**, 718. Oldano, C., 1986, *Phys. Rev. Lett.*, **56**, 1098. Miraldi, E., Oldano, C., and Strigazzi, A., 1986, *Phys. Rev.* A, **34**, 4348. Zimmermann, W., and Kramer, L., 1986, *Phys. Rev. Lett.*, **56**, 2655. Kini, U. D., 1986, *J. Phys., Paris*, **47**, 693; 1986, *Ibid*, **47**, 1829; 1987, *Ibid.*, **48**, 1187; 1988, *Ibid.*, **49**, 527.

[22] Madhusudana, N. V., and Durand, G., 1985, *J. Phys., Paris*, **46**, L195.

[23] Dozov, I., Martinot-Lagarde, Ph., and Durand, G., 1982, *J. Phys., Paris*, **43**, L365.

[24] Madhusudana, N. V., and Raghunathan, V. A., 1988, *Molec. Crystals liq. Crystals Lett.*, **5**, 201.

[25] Kai, S. (private communication).

[26] Barbero, G., Taverna Valabrega, T., Bartolino, R., and Valenti, B., 1986, *Liq. Crystals*, **1**, 483.

[27] Pesch, W., and Kramer, L., 1986, *Z. Phys.* B, **63**, 121.

[28] Kramer, L., Bodenschatz, E., Pesch, W., and Zimmermann, W., 1987, *The Physics of Structure Formation*, edited by W. Güttinger and G. Dangelmayr (Springer-Verlag), p. 130.

[29] BODENSCHATZ, E., 1985, Diploma thesis, Bayreuth.
[30] KAISER, M., 1988, Diploma thesis, Bayreuth. KAISER, M., and PESCH, W. (to be published).
[31] RASENAT, S., HARTUNG, G., WINKLER, B. L., and REHBERG, I., 1989, *Exp. Fluids*, **7**, 213.
[32] BODENSCHATZ, E., PESCH, W., and KRAMER, L., 1988, *Physica* D, **32**, 135.
[33] ECKHAUS, W., 1965, *Studies in Nonlinear Stability Theory* (Springer-Verlag), p. 93. NEWELL, A. C., and WHITEHEAD, J. A., 1969, *J. Fluid Mech.*, **38**, 279.
[34] KRAMER, L., and ZIMMERMANN, W., 1985, *Physica* D, **16**, 221.
[35] KRAMER, L., SCHOBER, H. R., and ZIMMERMANN, W., 1988, *Physica* D, **31**, 212.
[36] LOWE, M., and GOLLUB, J., 1985, *Phys. Rev. Lett.*, **55**, 2575.
[37] BODENSCHATZ, E., and KRAMER, L., 1987, *Physica* D, **27**, 249.
[38] POMEAU, Y., ZALESKI, S., and MANNEVILLE, P., 1983, *Phys. Rev.* A, **27**, 2710. TESAURO, G., and CROSS, M. C., 1986, *Phys. Rev.* A, **34**, 1363.
[39] GIL, L., and LEGA, J. (private communication).
[40] Yamazaki, H., Kai, S., and HIRAKAWA, K., 1987, *J. phys. Soc. Japan*, **56**, 1.
[41] RIBOTTA, R., and JOETS, A., 1984, *Cellular Structures in Instabilities*, edited by J. E. Wesfreid and S. Zaleski (Springer-Verlag), p. 249.
[42] JOETS, A., and RIBOTTA, R., 1988, *Phys. Rev. Lett.*, **60**, 2164.
[43] KRAMER, L., ZIMMERMANN, W., BODENSCHATZ, E., and PESCH, W., 1988, *Propagation in Systems Far From Equilibrium*, edited by J. E. Wesfreid *et al.* (Springer-Verlag), p. 240.
[44] ZIPPELIUS, A., and SIGGIA, E. D., 1983, *Phys. Fluids*, **26**, 2905. CROSS, M. C., 1983, *Phys. Rev.* A, **27**, 490. BUSSE, F. H., and BOLTON, E. W., 1984, *J. Fluid Mech.*, **146**, 115.
[45] SHIWA, Y., and KAWASAKI, K., 1986, *J. Phys.* A, **19**, 1387.